

*Original Research*

# Magnetic Resonance Imaging Combined with Histological Techniques for Dynamic Assessment of Cytotoxic Edema after Cerebral Ischemia-Reperfusion Injury

Yuhui Ma<sup>1,2,†</sup>, Peilun Xiao<sup>3,†</sup>, Chenmeng Liu<sup>2</sup>, Haimo Zhang<sup>2</sup>, Zhen Li<sup>1,2</sup>, Chen Li<sup>2</sup>, Miao Yu<sup>2</sup>, Jinfeng Long<sup>2</sup>, Lin An<sup>2,\*</sup>, Xizhen Wang<sup>1,\*</sup>, Xiaoli Wang<sup>1,2,\*</sup><sup>1</sup>Medical Imaging Center, Affiliated Hospital of Weifang Medical University, 261053 Weifang, Shandong, China<sup>2</sup>School of Medical Imaging, Weifang Medical University, 261053 Weifang, Shandong, China<sup>3</sup>Department of Anatomy, School of Basic Medicine, Weifang Medical University, 261053 Weifang, Shandong, China\*Correspondence: [wranlin@163.com](mailto:wranlin@163.com) (Lin An); [wangxizhen@wfmuc.edu.cn](mailto:wangxizhen@wfmuc.edu.cn) (Xizhen Wang); [wxlpine@wfmuc.edu.cn](mailto:wxlpine@wfmuc.edu.cn) (Xiaoli Wang)

†These authors contributed equally.

Academic Editor: Jesús Pastor

Submitted: 18 June 2023 Revised: 21 September 2023 Accepted: 25 September 2023 Published: 8 November 2023

## Abstract

**Background:** Reperfusion therapy after ischemic cerebral stroke may cause cerebral ischemia-reperfusion injury (CIRI), and cerebral edema is an important factor that may aggravate CIRI. Our study aimed to dynamically monitor the development of early cytotoxic edema after CIRI by magnetic resonance imaging (MRI) and to validate it using multiple histological imaging methods. **Methods:** Male Sprague Dawley rats were divided into sham and CIRI groups. T2-weighted imaging (T2WI) and diffusion-weighted imaging (DWI)-MRI scans were performed in the sham and CIRI groups after reperfusion. Relative apparent diffusion coefficient (rADC) values were calculated and the midline shift (MLS) was measured. A series of histological detection techniques were performed to observe changes in the cerebral cortex and striatum of CIRI rats. Correlation analysis of rADC values with aquaporin-4 (AQP4) and sodium-potassium-chloride cotransport protein 1 (Na<sup>+</sup>-K<sup>+</sup>-2Cl<sup>-</sup>-cotransporter 1; NKCC1) was performed. **Results:** rADC values began to increase and reached a relatively low value in the cerebral cortex and striatum at 24 h after reperfusion, and the MLS reached relatively high values at 24 h after reperfusion (all  $p < 0.05$ ). Hematoxylin-eosin (HE) staining showed that the nerve cells in the cortex and striatum of the sham group were regular in morphology and neatly arranged, and in the CIRI-24 h group were irregular, disorganized, and loosely structured. Using terminal deoxynucleotidyl transferase dUTP nick end labeling (TUNEL) staining, the number of TUNEL<sup>+</sup> cells in the ischemic cortex and striatum in CIRI-24 h group was shown to increase significantly compared with the sham group ( $p < 0.05$ ). Transmission electron microscopy showed that the perivascular astrocytic foot processes were swollen in the cortex and striatum of the CIRI-24 h group. Pearson correlation analysis demonstrated that rADC values were negatively correlated with the number of anti-gliabryllary acidic protein (GFAP)<sup>+</sup>AQP4<sup>+</sup> and GFAP<sup>+</sup>NKCC1<sup>+</sup> cells of the CIRI rats. **Conclusions:** MRI combined with histological techniques can dynamically assess cytotoxic edema after CIRI, in a manner that is clear and intuitive for scientific researchers and clinicians, and provides a scientific basis for the application of MRI techniques for monitoring the dynamic progress of CIRI.

**Keywords:** cerebral ischemia-reperfusion injury; stroke; magnetic resonance imaging; cytotoxic edema; rat

## 1. Introduction

With an increasingly aging population worldwide, the prevalence of ischemic stroke is also gradually increasing [1]. While early intravenous thrombolysis or vascular intervention for embolization can save brain tissue on the verge of necrosis, it also can lead to cerebral ischemia-reperfusion injury (CIRI) [2]. Cerebral edema is an important factor that may aggravate CIRI [3]. Attention to brain edema progression and cytotoxic edema stages is important for improving patient prognosis [4,5].

Magnetic resonance imaging (MRI) is a promising tool and a key component of numerous treatments and diagnostics, providing relatively stable and reproducible results [6]. Studies have shown that T2-weighted imaging (T2WI) and diffusion-weighted imaging (DWI)-MRI can be used as

reliable diagnostic methods to clinically determine the status of cerebral edema in patients with CIRI, providing reference information for determining subsequent treatment options [7]. However, dynamic monitoring of CIRI patients has some limitations in clinical practice.

Astrocytes are the most abundant cell type in the mammalian brain, and astrocyte swelling is the most important component of the early cytotoxic brain edema state after CIRI [8]. Cytoplasmic membranes of astrocytes are rich in water flux channels such as aquaporin-4 (AQP4) [9] and sodium-potassium-chloride cotransport protein 1 (Na<sup>+</sup>-K<sup>+</sup>-2Cl<sup>-</sup>-cotransporter 1; NKCC1) [10]. Extracellular water enters the cells early in CIRI, triggering cellular swelling, which can further rupture cell membranes, leading to cell rupture and death [11]. As this process occurs mainly in astrocytes, astrocytic edema is an important cause



and marker of cytotoxic edema [12]. Histological analysis remains the basis for assessing pathological alterations after CIRI [13], and pathological tissue section staining allows observation of changes in membrane permeability-related proteins, such as AQP4 and NKCC1, that can be used as the gold standard for monitoring changes in brain cell membrane permeability [14].

Clinical and translational studies have proved the ability of T2WI and DWI to monitor edema content and evolution [15]. However, the dynamic evolution of cerebral edema, especially in the acute phase, is not fully understood. Therefore, in the present study, we applied T2WI and DWI-MRI methods to continuously and dynamically monitor the cerebral cortex and striatum of CIRI rats to quantitatively assess the alterations of cytotoxic edema, and compared *in vivo* images with histopathological results for a more in-depth analysis to understand the progression of cytotoxic edema after CIRI.

## 2. Materials and Methods

### 2.1 Animals and Treatment

Specific-pathogen-free healthy adult male Sprague Dawley rats (8 weeks old; 250–280 g; Jinan Pengyue Laboratory Animal Breeding Co., Jinan, Shandong, China; animal license: SCXK (Lu) 20220006) were housed under a 12 h light/dark cycle ( $22 \pm 1$  °C, 40–60 % humidity). The rats were randomly divided into six groups: one sham group and five CIRI groups, namely CIRI-2 h, 6 h, 12 h, 24 h, and 72 h according to the time after reperfusion. A modified Zea-Longa wire embolization method was used to prepare a middle cerebral artery occlusion (MCAO) model [16]. A wire plug ( $0.34 \pm 0.02$  mm) was inserted into the right common carotid artery (CCA), with the plug head entering the internal carotid artery (ICA) and stopping at a distance of approximately 18.0 mm from the bifurcation of the CCA. Two hours later, the wire was removed for reperfusion. Only the right CCA was isolated in the rats of the sham group. The experimental design of the study is outlined in Fig. 1.

### 2.2 Behavioral Tests

The neurological examination of CIRI rats was performed at CIRI-2 h according to the Longa scale [16]. Neurological findings were graded on a five-point scale: 0, no neurological deficit; 1, mild focal neurologic deficit with the inability to extend the left forefoot; 2, moderate focal neurologic deficit with circling to the left; 3, severe focal deficit with falling to the left; and 4, inability to walk spontaneously and depressed level of consciousness. Scores of 1–3 were selected for inclusion in the study.

### 2.3 MRI Data Acquisition

MRI examination was performed using a 7.0 T MRI scanner (BioSpec 70/20 USR; Bruker, Karlsruhe, Germany). Anesthesia was induced by a small animal anesthe-

sia machine (R500, RWD, Shenzhen, Guangdong, China) using a mixture of 5% isoflurane and 95% oxygen, and maintained by a mixture of 2% isoflurane and 98% oxygen. The rats were placed in the center of the magnetic field. The regions of interest (ROIs) were outlined in the cerebral cortex and striatum. All ROI analyses were carried out in the ischemic right hemisphere and in the contralateral left hemisphere using the image analysis software ImageJ (ImageJ 1.6.0, National Institutes of Health, <https://imagej.net/ij/index.html>, Bethesda, MD, USA).

### 2.4 T2WI

T2-weighted images were collected using a spin-echo sequence with the following parameters: TR (repetition time) = 3000 ms, TE (echo time) = 34 ms, FOV (field of view) =  $3.3 \times 3.1$  cm<sup>2</sup>, MTX (matrix size) =  $160 \times 150$ , and ST (slice thickness) = 0.5 mm. The midline shift (MLS) quantification method was used to determine the space-occupying effect of the cerebral edema. The largest level of the lateral ventricle was selected. The distance between the outer margin of the cortex and the middle of the lateral ventricle was measured from the ipsilateral (a) and contralateral (b) sides. The calculation formula is as follows:  $MLS = (a-b) / 2$  [17].

### 2.5 DWI

The DWI parameters were: TR = 3000 ms, TE = 22 ms, FOV =  $3.0 \times 3.0$  cm<sup>2</sup>, MTX =  $128 \times 128$ , ST = 0.8 mm, and b-value of 0, 1000 s/mm<sup>2</sup>. Image processing was performed using small animal MRI workstation image post-processing software to generate apparent diffusion coefficient (ADC) maps. The largest level of the lateral ventricle of the coronal ADC map was selected, and the ischemic side of the cerebral cortex and striatum were manually drawn on the ADC map, as well as the contralateral mirror area as the ROI. ADC values were obtained from each ROI, and its relative mean value was calculated and expressed as the ipsilateral ADC compared with the contralateral ADC values [18].

### 2.6 Specimen Collection and Processing

After MRI scans, all rats were injected with sodium pentobarbital (cat# P3761-5G; 58 mg/kg; Sigma-Aldrich, St. Louis, MO, USA) and subsequently perfused with physiological saline and 4% paraformaldehyde (PFA) through the heart. The brain was removed and fixed in PFA for 24 h. Brain tissue was embedded in paraffin wax. The lateral ventricular level (2.2 mm anterior to 0.26 mm posterior to the bregmatic fontanelle) was localized and sliced using a paraffin slicer (Finesse 325; Thermo Scientific, Waltham, MA, USA) to make 4- $\mu$ m-thick sections.

### 2.7 TUNEL Assay

The paraffin sections were waxed, hydrated, and stained using a terminal deoxynucleotidyl transferase dUTP

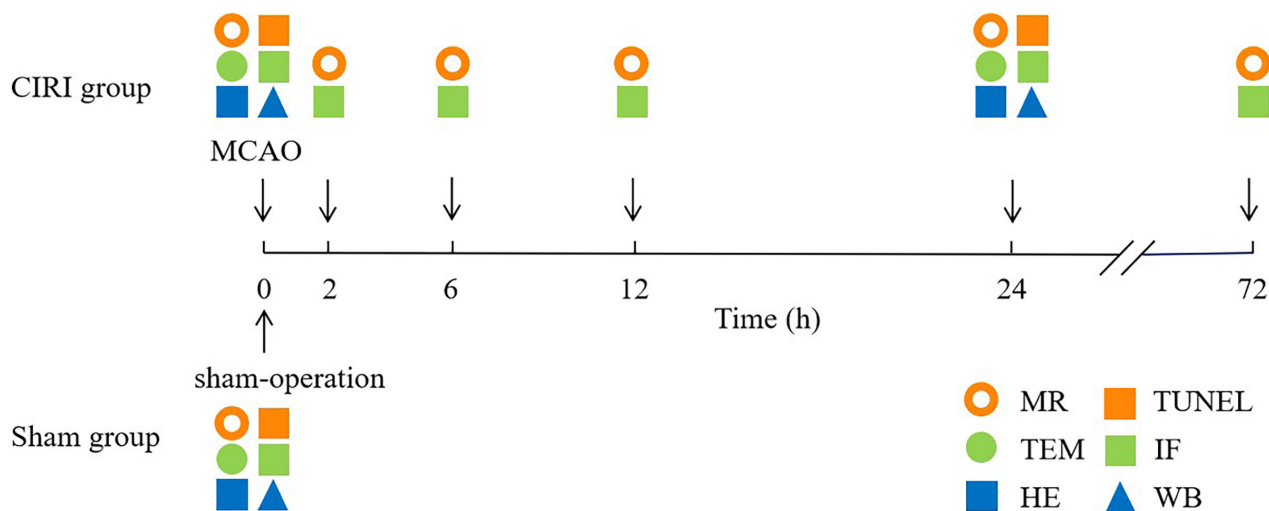


**Fig. 1. Experiment design.** Experimental timeline of the sham and CIRI groups, which underwent sham or MCAO operation, and a series tests of MR examination, TEM scans, HE staining, TUNEL staining, IF staining, and WB analysis were performed. CIRI, cerebral ischemia-reperfusion injury; IF, immunofluorescence; HE, hematoxylin-eosin; MCAO, middle cerebral artery occlusion; MR, magnetic resonance; TEM, transmission electron microscopy; TUNEL, terminal deoxynucleotidyl transferase dUTP nick end labeling; WB, western blot.

nick end labeling (TUNEL) kit (MK1014-100; Boster, Wuhan, Hubei, China), according to the manufacturer's instructions. The sections were then observed and photographed under an upright optical microscope (BX51; Olympus, Tokyo, Japan). TUNEL<sup>+</sup> cell counts were recorded as cells/mm<sup>2</sup>, and the mean value was adopted.

### 2.8 HE Staining

Paraffin sections of brain tissue were baked at a constant temperature of 60 °C for 1 h. The sections were then dewaxed using xylene, hydrated using gradient ethanol, and stained sequentially with hematoxylin-eosin (HE) (G1120; Solarbio, Beijing, China). The sections were then dehydrated in anhydrous ethanol and cleaned in xylene. Finally, the sections were sealed with neutral gum. The morphological changes of cells were observed under an upright optical microscope (BX51; Olympus, Tokyo, Japan).

### 2.9 TEM

After anesthesia, rats were perfused with 4% PFA and 2.5% glutaraldehyde buffer (pH 7.4). Brain tissue specimens were collected, and cerebral cortex and striatum on the ischemic side were separated and cut into small pieces (1 × 1 × 1 mm<sup>3</sup>). Specimens were fixed in 1% osmium tetroxide, dehydrated through gradient ethanol, then embedded in epoxy resin. 40-nm thick sample sections were placed on a 200-mesh copper grid, stained with saturated uranyl acetate and lead citrate, then visualized using transmission electron microscopy (TEM) (HT-7700; Hitachi, Tokyo, Japan).

### 2.10 IF Staining

Immunofluorescence (IF) staining was performed on sections obtained from the sham and CIRI groups. Brain tissue sections were dewaxed and hydrated sequentially, and antigen repair was performed by the water bath thermal repair method. Rabbit anti-AQP4 (16473-1-AP, 1:1000; Proteintech, Wuhan, Hubei, China) and mouse anti-gial fibrillary acidic protein (GFAP) (3670S, 1:300; Cell Signaling Technology, Danvers, MA, USA) primary antibody mixture or rabbit anti-NKCC1 (13884-1-AP, 1:80; Proteintech) and mouse anti-GFAP primary antibody mixture were added as needed, and refrigerated at 4 °C overnight. On the next day, goat anti-rabbit IgG (ZF-0511, 1:200; Zhongshan Golden Bridge Biology Company, Beijing, China) and goat anti-mouse IgG (ZF-0513, 1:200; Zhongshan Golden Bridge Biology Company) fluorescent secondary antibody mixes were added, incubated for 1 h and protected from light, and the slices were sealed with fluorescent blocker containing 4',6-diamidino-2-phenylindole (DAPI) solution (F6057-20ML; Sigma-Aldrich, St. Louis, MO, USA). The slices were observed and photographed under an upright fluorescent microscope (AxioLab 5; Zeiss, Oberkochen, Germany). The number of GFAP<sup>+</sup>/AQP4<sup>+</sup> and GFAP<sup>+</sup>/NKCC1<sup>+</sup> cells were counted as cells/mm<sup>2</sup>, and the mean values were calculated.

### 2.11 Western Blot (WB) Analysis

Protein concentrations were quantified separately using a bicinchoninic acid protein assay reagent kit

(20201ES86, YEASEA, Shanghai, China). After transferring the proteins to the polyvinylidene fluoride membrane, and the membranes were blocked with 5% non-fat milk powder for 2 h. The strips were incubated in rabbit anti-AQP4 (16473-1-AP, 1:5000; Proteintech, Wuhan, Hubei, China) primary antibody, rabbit anti-NKCC1 (13884-1-AP, 1:1000; Proteintech, Wuhan, Hubei, China) primary antibody, and mouse anti  $\beta$ -tubulin (2128S 1:10,000; Cell Signaling Technology, Danvers, MA, USA) primary antibody and incubated overnight at 4 °C. The next day, goat anti-rabbit (SA00001-2, 1:10,000; Proteintech, Wuhan, Hubei, China) or goat anti-mouse (SA00001-1, 1:10,000; Proteintech, Wuhan, Hubei, China) secondary antibody was added and incubated at room temperature for 2 h. The proteins were exposed and photographed using a high-performance imaging system, and the relative expression of each protein was analyzed using ImageJ software.

### 2.12 Statistical Analysis

Statistical analyses were performed using SPSS 22.0 software (SPSS Inc., Chicago, IL, USA). Shapiro Wilk analysis was used to verify the normality of the measured data, and all normally distributed data are represented as mean  $\pm$  standard deviation. MRI data were compared using repeated measures analysis of variance (RMANOVA). Histological data were compared using one way analysis of variance (ANOVA) and further compared using the least significant difference (LSD) test. For correlation analysis, we adopted a method of combining Pearson's correlation analysis and general linear regression analysis. Statistical significance was set at  $p < 0.05$ .

## 3. Results

### 3.1 Comparison of Brain Tissues in the Sham and CIRI Groups Based on MRI

T2WI (Fig. 2A) and DWI-MRI (Fig. 2B,C) scans indicated that the brain tissue of the sham group rats had uniform signal and bilateral symmetry, and no abnormal signals were observed. At CIRI-2 h, abnormal signal areas of cerebral edema appeared in the cerebral hemisphere on the ischemic side of the CIRI group, the midline of the brain was shifted to the contralateral side, and the relative apparent diffusion coefficient (rADC) values of the cerebral cortex and striatum decreased compared with the sham group. The midline of the brain was further shifted to the contralateral side at CIRI-6 h and 12 h, and the rADC values were lower than before. At CIRI-24 h, extensive cerebral edema was seen in the cerebral hemisphere on the ischemic side of the CIRI group, the MLS was relatively large, and the rADC value reached a relatively low level. At CIRI-72 h, the MLS was reduced and the rADC value was increased compared to that at CIRI-24 h (Fig. 2D–F, all  $*p < 0.05$ ,  $n = 6$ ).

### 3.2 Changes in the Cerebral Cortex and Striatum in CIRI Rats Assessed by HE Staining

HE staining showed that the nerve cells in the cortex and striatum of the sham group were regular in morphology and neatly arranged. At CIRI-24 h, the nerve cells had irregular morphology, disorganized arrangement, and loose structure, and some nuclei were deeply stained (Fig. 3A,  $n = 6$ ).

### 3.3 Changes in the Cerebral Cortex and Striatum in CIRI Rats Assessed by TUNEL Staining

TUNEL assay showed that TUNEL<sup>+</sup> cells were occasionally observed in the cortex and striatum in the sham group. However, the CIRI-24 h group showed a significantly increased number of TUNEL<sup>+</sup> cells in the ischemic cortex and striatum (Fig. 3B,C,  $*p < 0.05$ ,  $n = 6$ ).

### 3.4 Changes in the Cerebral Cortex and Striatum in CIRI Rats Assessed by TEM

The perivascular astrocytic foot processes (APs) in the cerebral cortex and striatum were relatively thin and flat in the sham group, and the perivascular astrocytic APs were enlarged on the ischemic side of the CIRI-24 h group (Fig. 4,  $n = 6$ ).

### 3.5 Changes in the Cerebral Cortex and Striatum in CIRI Rats Assessed by IF Staining

IF double-label staining showed that the number of GFAP<sup>+</sup>/NKCC1<sup>+</sup> (Fig. 5A) and GFAP<sup>+</sup>/AQP4<sup>+</sup> (Fig. 5B) double-positive cells in the cortex and striatum of the ischemic side in the CIRI groups were significantly different compared with those in the sham group (Fig. 5C–E  $*p < 0.05$ ,  $n = 6$ ). Moreover, the number of these two double-positive cells in the ischemic side of the cortex in the CIRI-2 h group was significantly higher than that in the sham group (Fig. 5C,D,  $*p < 0.05$ ,  $n = 6$ ). However, the cell number in the striatum was not significantly different to the sham group. The expression of these two cells on the ischemic side of the cortex in the CIRI group increased at 2 h after reperfusion when compared with the sham group. However, in the striatum, this increased at 6 h after reperfusion. The double-positive cell number peaked at 24 h after reperfusion in the ischemic side of the cortex and at 12 h after reperfusion in the ischemic side of the striatum. The number of double-positive cells was decreased at 72 h after reperfusion compared with 24 h after reperfusion in the ischemic side of the cortex, but were increased in the striatum (Fig. 5C,D,  $*p < 0.05$ ,  $n = 6$ ).

### 3.6 Changes in the Cerebral Cortex and Striatum in CIRI Rats Assessed by WB

According to western blot (WB) measurements, the expression of AQP4 and NKCC1 protein in the ischemic cortex (Fig. 6A) and striatum (Fig. 6B) was significantly higher in the CIRI-24 h groups than in the sham group (Fig. 6C,D,  $*p < 0.05$ ,  $n = 3$ ).

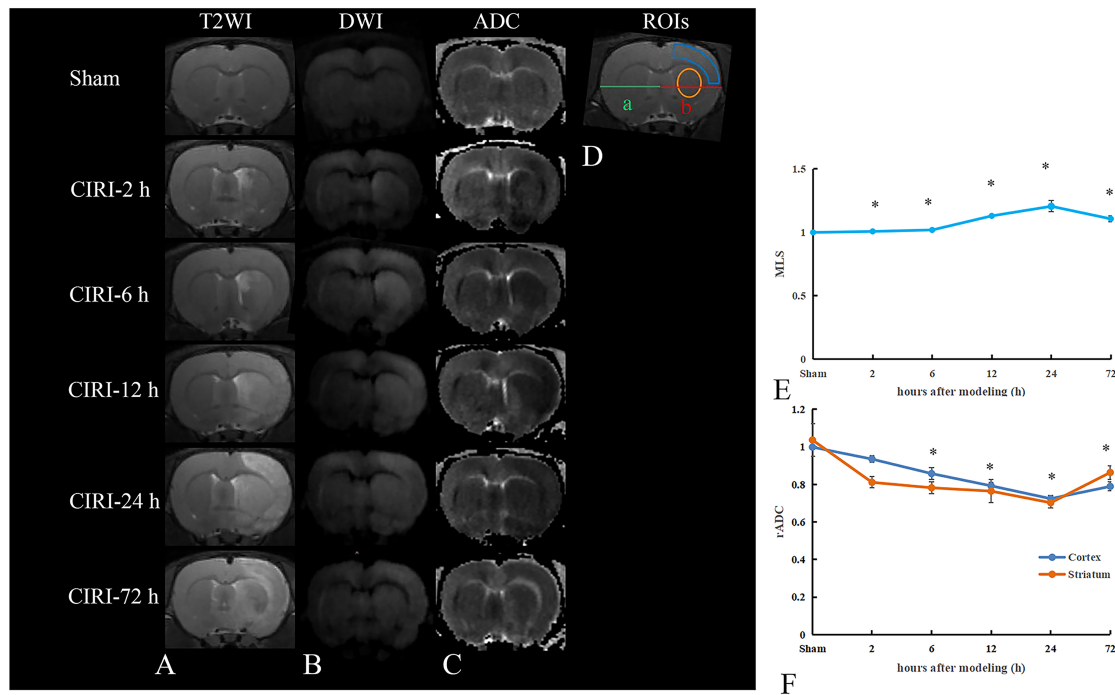


**Fig. 2. Dynamic multimodal MRI results.** (A) T2WI images of the sham and CIRI groups. (B) DWI images of the sham and CIRI groups. (C) ADC images of the sham and CIRI groups. (D) Schematic diagram of the ROIs of the cortex and striatum and computation of MLS. (E) Analysis of the relative MLS in the sham and CIRI groups. (F) Analysis of the rADC in the sham and CIRI groups. Data are presented as mean  $\pm$  standard deviation. \* $p < 0.05$  vs. sham group. ADC, apparent diffusion coefficient; DWI, diffusion weighted imaging; MLS, midline shift; rADC, relative apparent diffusion coefficient; ROIs, regions of interest; T2WI, T2-weighted imaging.

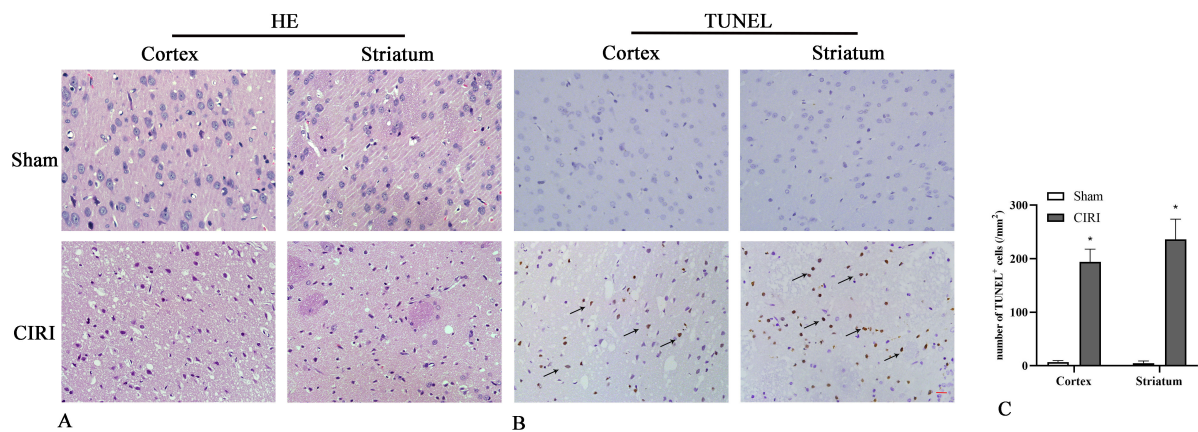


**Fig. 3. The results of HE and TUNEL staining in the sham and CIRI-24 h groups.** (A) HE images of the sham and CIRI groups. (B) TUNEL images of the sham and CIRI groups. (C) Analysis of the number of TUNEL<sup>+</sup> cells. Data are presented as mean  $\pm$  standard deviation. \* $p < 0.05$  vs. sham group. Scale bar = 20  $\mu$ m.

### 3.7 Correlation of rADC Value with GFAP<sup>+</sup>/AQP4<sup>+</sup> and GFAP<sup>+</sup>/NKCC1<sup>+</sup> Cells

Pearson's correlation analysis and general linear regression showed that at each time point after reperfusion, the number of GFAP<sup>+</sup>/AQP4<sup>+</sup> (Fig. 7A) and GFAP<sup>+</sup>/NKCC1<sup>+</sup> (Fig. 7C) cells on the ischemic side of

the cerebral cortex showed a statistically significant negative correlation with rADC. The number of GFAP<sup>+</sup>/AQP4<sup>+</sup> (Fig. 7B) and GFAP<sup>+</sup>/NKCC1<sup>+</sup> (Fig. 7D) cells on the ischemic side of the striatum showed a moderate negative correlation with rADC (Fig. 7, all  $p < 0.01$ ,  $n = 6$ ).

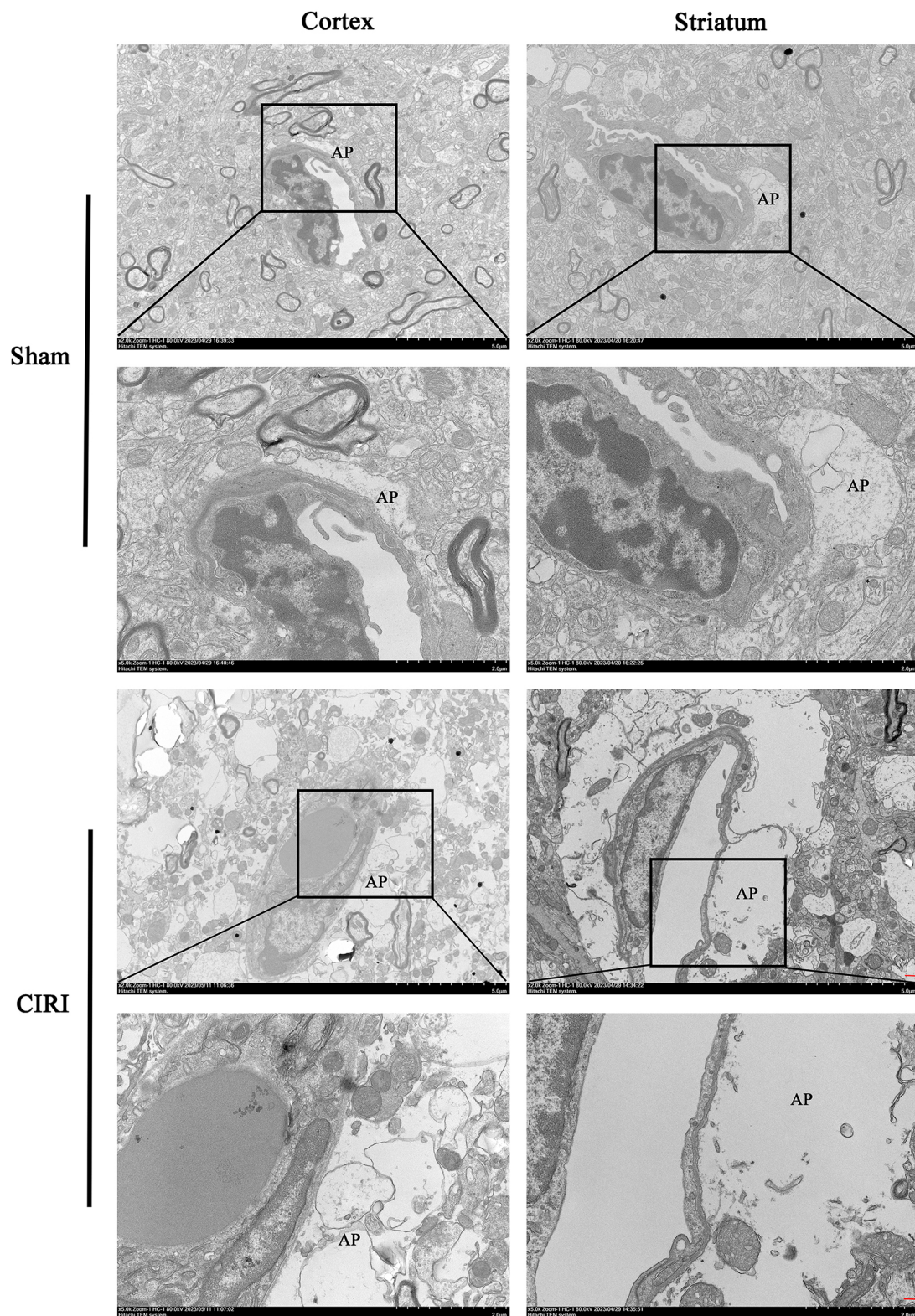


**Fig. 4. TEM images of the sham and CIRI-24 h groups.** Enlarged areas indicates an AP. Scale bar = 5  $\mu\text{m}$  in 2000 $\times$  figures with rectangular markers, 2  $\mu\text{m}$  in 5000 $\times$  figures with no rectangular markers. AP, astrocytic foot process; TEM, transmission electron microscopy.

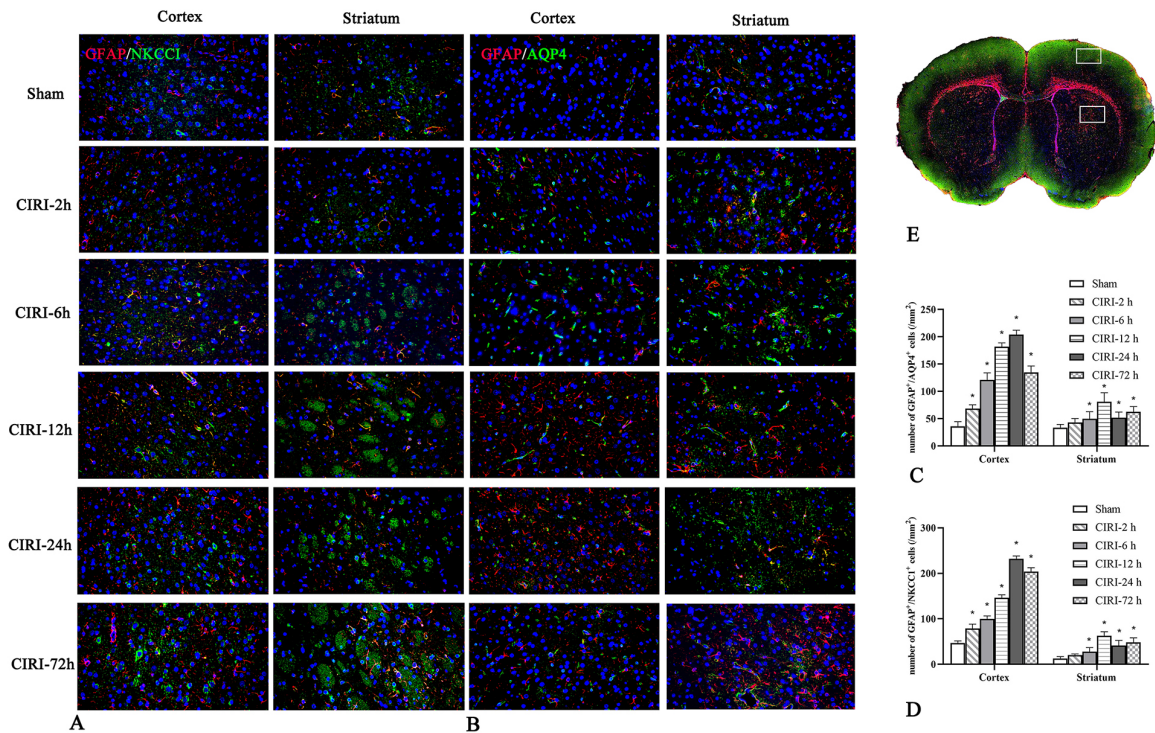


**Fig. 5.** IF staining of GFAP<sup>+</sup>/AQP4<sup>+</sup> and GFAP<sup>+</sup>/NKCC1<sup>+</sup> in the sham and CIRI groups. (A) GFAP<sup>+</sup>/AQP4<sup>+</sup> IF images of the sham and CIRI groups. (B) GFAP<sup>+</sup>/NKCC1<sup>+</sup> IF images of the sham and CIRI groups. (C) Analysis of the number of GFAP<sup>+</sup>/AQP4<sup>+</sup> cells. (D) Analysis of the number of GFAP<sup>+</sup>/NKCC1<sup>+</sup> cells. (E) Schematic diagram of the ROIs of the cortex and striatum. Data are presented as mean ± standard deviation. \**p* < 0.05 vs. sham group. Scale bar = 20 μm. AQP4, aquaporin-4; GFAP, glial fibrillary acidic protein; NKCC1, sodium-potassium-chloride cotransport protein 1.

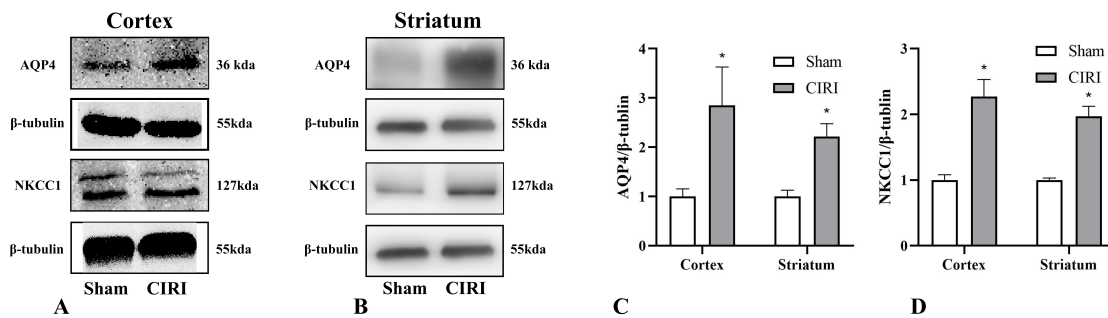


**Fig. 6.** WB analysis results of AQP4 and NKCC1 of the sham and CIRI-24 h groups. (A) WB images of AQP4 and NKCC1 in the ischemic cortex of the sham and CIRI-24 h groups. (B) WB images of AQP4 and NKCC1 in the ischemic striatum of the sham and CIRI-24 h groups. (C) Comparison of AQP4 protein expression in the sham and CIRI-24 h groups. (D) Comparison of NKCC1 protein expression in the sham and CIRI-24 h groups. Data are presented as mean ± standard deviation. \**p* < 0.05 vs. sham group.

#### 4. Discussion

Ischemic stroke is an increasingly serious public health problem [19]. Reperfusion therapy with thrombolysis or thrombus extraction has become the preferred method recommended by national guidelines [20], but the occurrence of cerebral edema after reperfusion can aggravate neurological impairment [21]. There is therefore an urgent

need to understand the dynamic progression of brain edema after CIRI to provide reliable information for clinical treatment [22].

In this study, we used MRI combined with multiple histological methods for the dynamic monitoring of brain edema after CIRI. We confirmed that the combined application of multi-scale and multi-parameter techniques can provide comprehensive information on CIRI rats. This is

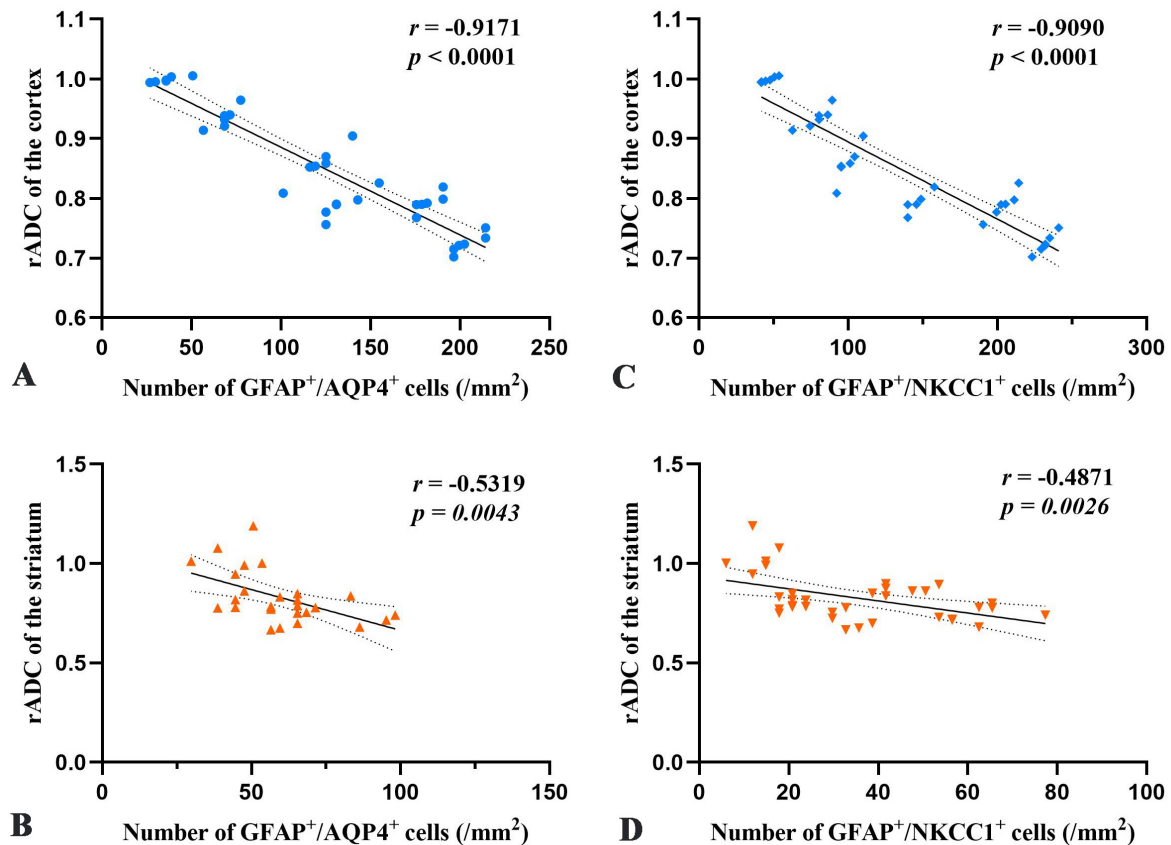


**Fig. 7. Correlation analysis of the number of GFAP<sup>+</sup>/AQP4<sup>+</sup> and GFAP<sup>+</sup>/NKCC1<sup>+</sup> cells with rADC value in the sham and CIRI groups at each time point after reperfusion.** (A) Correlation analysis of rADC and the number of GFAP<sup>+</sup>/AQP4<sup>+</sup> cells in the cortex. (B) Correlation analysis of rADC and the number of GFAP<sup>+</sup>/NKCC1<sup>+</sup> cells in the cortex. (C) Correlation analysis of rADC and the number of GFAP<sup>+</sup>/AQP4<sup>+</sup> cells in the striatum. (D) Correlation analysis of rADC and the number of GFAP<sup>+</sup>/NKCC1<sup>+</sup> cells in the striatum. Blue and orange colors indicate cortex and striatum data, respectively. AQP4, aquaporin-4; GFAP, glial fibrillary acidic protein; NKCC1, sodium-potassium-chloride cotransport protein 1; rADC, relative apparent diffusion coefficient.

not only beneficial for exploring the pathophysiological changes in local lesions of brain diseases such as CIRI [23] but also helpful for improving our understanding and clinical prevention [24]. Specifically, our MRI images showed significant enlargement of ischemic lesions in CIRI rats from the acute phase, which reached comparable severity at CIRI-24 h and then decreased. In addition, histologically, AQP4 and NKCC1 were closely associated with astrocytotoxic edema.

T2WI is commonly used to assess vasogenic edema and infarct area after CIRI [25], and the ADC value of DWI, a quantitative parameter, reflects the degree of diffusion restriction of water molecules due to cytotoxic edema [26]. To summarize, we believe that MRI has high application value in CIRI, although histological methods are still needed to determine the accuracy and sensitivity of diagnoses [27]. AQP4, which is mainly expressed in astrocytes, plays a key role in maintaining water balance, osmoregulation, energy metabolism, and cytotoxic edema after CIRI

[28]. NKCC1 is also an important transporter protein for astrocyte volume regulation, and its activation causes intracellular osmotic solute accumulation and co-transport of water molecules into the cell, leading to cytotoxic edema [29].

Our TEM results demonstrated that cytotoxic edema in the ischemic cortex and striatum occurred mainly in astrocytes, in accordance with a previous study [30]. Other studies have found that AQP4 [31] and NKCC1 [32] both play crucial roles in early edema development following ischemia; however, this has not been the subject of a continuous dynamic observational study. The results of our study showed that the astrocyte water channel protein AQP4 and transporter protein NKCC1 expression increased in the ischemic side of the brain in CIRI rats and reached a relatively high level at 24 h in the cortex and at 12 h in the striatum. These results show that changes in the expression of brain edema-related proteins AQP4 and NKCC1 are closely related to astrocytic toxic edema. Moreover, correlation anal-

yses showed that AQP4 and NKCC1 were negatively correlated with the quantitative parameter rADC values in the cortex and striatum. The above results verified the feasibility of using MRI combined with histologic multiscale imaging to monitor early cytotoxic edema after CIRI.

Our study also had some limitations. Cytotoxic edema was determined and evaluated by T2WI, DWI, and ADC-MRI combined with histological techniques from 2 h to 72 h after CIRI; however, further timepoints may need to be explored, and observations performed over a longer period of time.

## 5. Conclusions

Our results confirm that MRI combined with histological techniques can dynamically assess the progression of cytotoxic edema after CIRI in a clear and intuitive manner, and provide a scientific and theoretical basis for researchers and clinicians regarding the application of MRI techniques in this disease.

## Abbreviations

CIRI, cerebral ischemia-reperfusion injury; MRI, magnetic resonance imaging; T2WI, T2-weighted imaging; DWI, diffusion-weighted imaging; ADC, apparent diffusion coefficient; rADC, relative apparent diffusion coefficient; AQP4, aquaporin-4; NKCC1, sodium-potassium-chloride cotransport protein 1; GFAP, anti-gial fibrillary acidic protein; WB, western blot; HE, hematoxylin-eosin; TUNEL, terminal deoxynucleotidyl transferase dUTP nick end labeling; TEM, transmission electron microscopy; IF, immunofluorescence.

## Availability of Data and Materials

The raw data supporting the conclusion of this article will be made available by the authors, without undue reservation.

## Author Contributions

XLW and LA conceived the design of the project. YHM and PLX contributed to writing and editing the manuscript. YHM performed the data analysis. YHM, CL, JFL, CML, and HMZ performed the experiments. PLX and HMZ contributed to the preparation of the MCAO animal model. XZW performed the magnetic resonance imaging. ZL and MY provided access to behavioral equipment and participated in behavioral testing. XLW supervised the project. All authors contributed to editorial changes in the manuscript. All authors read and approved the final manuscript. All authors have participated sufficiently in the work and agreed to be accountable for all aspects of the work.

## Ethics Approval and Consent to Participate

The experimental procedures described in this study conformed to the requirements of the Animal Research: Reporting of *In Vivo* Experiments (ARRIVE) guidelines and were approved by the ethics committee of Weifang Medical University (approval No. 2020SDL052).

## Acknowledgment

Not applicable.

## Funding

This work was supported by the National Natural Science Foundation of China (82071888), Natural Science Foundation of Shandong Province (ZR2020MH074; ZR2021MH351), Shandong Province Traditional Chinese Medicine Science and Technology Development Plan (2019-0417; Q-2023071), Shandong Province Science and Technology Development Plan (202009010562), Weifang City Science and Technology Development Plan (2021GX057, 2022YX042) and 2019 Young Creative Talent Induction Program for Higher Education Institutions.

## Conflict of Interest

The authors declare no conflict of interest. Lin An is currently the General Manager of Guangdong Weiren Meditech Co. Ltd, Foshan, Guangdong, China. He is a visiting professor hired by Weifang Medical University to provide us with technical support in this study. The animal experiments in our manuscript were conducted at Weifang Medical University and the instruments in the manuscript we used are all from Weifang Medical University. There is no conflict of interest with Guangdong Weiren Meditech Co. Ltd.

## References

- [1] Han L, Jiang C. Evolution of blood-brain barrier in brain diseases and related systemic nanoscale brain-targeting drug delivery strategies. *Acta Pharmaceutica Sinica B*. 2021; 11: 2306–2325.
- [2] Farr GW, Hall CH, Farr SM, Wade R, Detzel JM, Adams AG, *et al*. Functionalized Phenylbenzamides Inhibit Aquaporin-4 Reducing Cerebral Edema and Improving Outcome in Two Models of CNS Injury. *Neuroscience*. 2019; 404: 484–498.
- [3] Surugiu R, Burdusel D, Ruscu MA, Cercel A, Hermann DM, Cadenas IF, *et al*. Clinical Ageing. *Subcellular Biochemistry*. 2023; 103: 437–458.
- [4] Zeng X, Zhang YD, Ma RY, Chen YJ, Xiang XM, Hou DY, *et al*. Activated Drp1 regulates p62-mediated autophagic flux and aggravates inflammation in cerebral ischemia-reperfusion via the ROS-RIP1/RIP3-exosome axis. *Military Medical Research*. 2022; 9: 25.
- [5] Du J, Yin G, Hu Y, Shi S, Jiang J, Song X, *et al*. Coicis semen protects against focal cerebral ischemia-reperfusion injury by inhibiting oxidative stress and promoting angiogenesis via the TGF $\beta$ /ALK1/Smad1/5 signaling pathway. *Aging (Albany NY)*. 2020; 13: 877–893.
- [6] Li G, Zhang B, Zhang M, Liu Q, Luo J, Liao Q, *et al*. A non-invasive real-time monitoring system for cytotoxic brain edema

in post ischemic stroke based on near-field coupling. *Technology and Health Care*. 2021; 29: 963–978.

- [7] Feis RA, Bouts MJRJ, Panman JL, Jiskoot LC, Dopfer EGP, Schouten TM, *et al*. Single-subject classification of presymptomatic frontotemporal dementia mutation carriers using multimodal MRI. *NeuroImage: Clinical*. 2018; 20: 188–196.
- [8] Lafrenaye AD, Simard JM. Bursting at the Seams: Molecular Mechanisms Mediating Astrocyte Swelling. *International Journal of Molecular Sciences*. 2019; 20: 330.
- [9] Kitchen P, Salman MM, Halsey AM, Clarke-Bland C, MacDonald JA, Ishida H, *et al*. Targeting Aquaporin-4 Subcellular Localization to Treat Central Nervous System Edema. *Cell*. 2020; 181: 784–799.e19.
- [10] Löscher W, Kaila K. CNS pharmacology of NKCC1 inhibitors. *Neuropharmacology*. 2022; 205: 108910.
- [11] Wang C, Hu F. Long noncoding RNA SOX2OT silencing alleviates cerebral ischemia-reperfusion injury via miR-135a-5p-mediated NR3C2 inhibition. *Brain Research Bulletin*. 2021; 173: 193–202.
- [12] Zhang J, Wang Y, Zheng Z, Sun X, Chen T, Li C, *et al*. Intracellular ion and protein nanoparticle-induced osmotic pressure modify astrocyte swelling and brain edema in response to glutamate stimuli. *Redox Biology*. 2019; 21: 101112.
- [13] Mao Z, Tian L, Liu J, Wu Q, Wang N, Wang G, *et al*. Ligustilide ameliorates hippocampal neuronal injury after cerebral ischemia reperfusion through activating PINK1/Parkin-dependent mitophagy. *Phytomedicine*. 2022; 101: 154111.
- [14] Deffner F, Gleiser C, Mattheus U, Wagner A, Neckel PH, Fallier-Becker P, *et al*. Aquaporin-4 expression in the human choroid plexus. *Cellular and Molecular Life Sciences*. 2022; 79: 90.
- [15] Obenaus A, Badaut J. Role of the non-invasive imaging techniques in monitoring and understanding the evolution of brain edema. *Journal of Neuroscience Research*. 2022; 100: 1191–1200.
- [16] Longa EZ, Weinstein PR, Carlson S, Cummins R. Reversible middle cerebral artery occlusion without craniectomy in rats. *Stroke*. 1989; 20: 84–91.
- [17] Gerriets T, Walberer M, Ritschel N, Tschernatsch M, Mueller C, Bachmann G, *et al*. Edema formation in the hyperacute phase of ischemic stroke. Laboratory investigation. *Journal of Neurosurgery*. 2009; 111: 1036–1042.
- [18] Seo HS, Na DG, Kim JH, Kim KW, Son KR. Correlation between CT and diffusion-weighted imaging of acute cerebral ischemia in a rat model. *American Journal of Neuroradiology*. 2011; 32: 728–733.
- [19] Jiang J, Dai J, Cui H. Vitexin reverses the autophagy dysfunction to attenuate MCAO-induced cerebral ischemic stroke via mTOR/Ulk1 pathway. *Biomedicine and Pharmacotherapy*. 2018; 99: 583–590.
- [20] Chen H, Guan B, Wang B, Pu H, Bai X, Chen X, *et al*. Glycyrrhizin Prevents Hemorrhagic Transformation and Improves Neurological Outcome in Ischemic Stroke with Delayed Thrombolysis Through Targeting Peroxynitrite-Mediated HMGB1 Signaling. *Translational Stroke Research*. 2020; 11: 967–982.
- [21] Datta A, Sarmah D, Kaur H, Chaudhary A, Mounica KL, Kalia K, *et al*. Post-stroke Impairment of the Blood-Brain Barrier and Perifocal Vasogenic Edema Is Alleviated by Endovascular Mesenchymal Stem Cell Administration: Modulation of the PKC $\delta$ /MMP9/AQP4-Mediated Pathway. *Molecular Neurobiology*. 2022; 59: 2758–2775.
- [22] Zhao Z, Zhang W, Zhang Y, Zhao Y, Zheng C, Tian H, *et al*. Multimodal Magnetic Resonance Imaging and Therapeutic Intervention With Yi-nao-jie-yu Decoction in a Rat Model of Post-stroke Depression. *Frontiers in Psychiatry*. 2020; 11: 557423.
- [23] Kim KA, Kim D, Kim JH, Shin YJ, Kim ES, Akram M, *et al*. Autophagy-mediated occludin degradation contributes to blood-brain barrier disruption during ischemia in bEnd.3 brain endothelial cells and rat ischemic stroke models. *Fluids and Barriers of the CNS*. 2020; 17: 21.
- [24] Guo P, Jin Z, Wu H, Li X, Ke J, Zhang Z, *et al*. Effects of irisin on the dysfunction of blood-brain barrier in rats after focal cerebral ischemia/reperfusion. *Brain and Behavior*. 2019; 9: e01425.
- [25] Huang YC, Tzeng WS, Wang CC, Cheng BC, Chang YK, Chen HH, *et al*. Neuroprotective effect of agmatine in rats with transient cerebral ischemia using MR imaging and histopathologic evaluation. *Magnetic Resonance Imaging*. 2013; 31: 1174–1181.
- [26] Sun C, Lin L, Yin L, Hao X, Tian J, Zhang X, *et al*. Acutely Inhibiting AQP4 With TGN-020 Improves Functional Outcome by Attenuating Edema and Peri-Infarct Astroglia After Cerebral Ischemia. *Frontiers in Immunology*. 2022; 13: 870029.
- [27] Gräfe D, Päts A, Merkschlagler A, Roth C, Hirsch FW, Frahm J, *et al*. STEAM-DWI as a robust alternative to EPI-DWI: Evaluation in pediatric brain MRI. *PLoS One*. 2022; 17: e0268523.
- [28] Vandebroek A, Yasui M. Regulation of AQP4 in the Central Nervous System. *International Journal of Molecular Sciences*. 2020; 21:1603.
- [29] Wang G, Huang H, He Y, Ruan L, Huang J. Bumetanide protects focal cerebral ischemia-reperfusion injury in rat. *International Journal of Clinical and Experimental Pathology*. 2014; 7: 1487–1494.
- [30] Liang D, Bhatta S, Gerzanich V, Simard JM. Cytotoxic edema: mechanisms of pathological cell swelling. *Neurosurgical Focus*. 2007; 22: E2.
- [31] Sucha P, Hermanova Z, Chmelova M, Kirdajova D, Camacho Garcia S, Marchetti V, *et al*. The absence of AQP4/TRPV4 complex substantially reduces acute cytotoxic edema following ischemic injury. *Frontiers in Cellular Neuroscience*. 2022;16:1054919.
- [32] Hertz L, Xu J, Chen Y, Gibbs ME, Du T, Hertz L, *et al*. Antagonists of the Vasopressin V1 Receptor and of the  $\beta(1)$ -Adrenoceptor Inhibit Cytotoxic Brain Edema in Stroke by Effects on Astrocytes - but the Mechanisms Differ. *Current Neuropharmacology*. 2014; 12: 308–323.